ISSN 0389-4010
UDC 533. 6. 011. 3

TECHNICAL REPORT OF NATIONAL AEROSPACE LABORATORY

TR-896T

Numerical Analysis of Inviscid Compressible Flows about Wing-Fuselage Combinations based on the Euler Equations

Tomiko ISHIGURO, Satoru OGAWA, and Keiko OGUCHI

May 1986

NATIONAL AEROSPACE LABORATORY

CHŌFU, TOKYO, JAPAN

Numerical Analysis of Inviscid Compressible Flows about Wing-Fuselage Combinations based on the Euler Equations*

Tomiko ISHIGURO**, Satoru OGAWA**
and Keiko OGUCHI**

ABSTRACT

A numerical procedure based on the Euler equations for analyzing the compressible inviscid transonic flow about a wing-fuselage combination is presented in this paper. In order to treat precisely boundary conditions on the combinational surface and at infinity, the exterior of the wing-fuselage combination in physical space is mapped into a rectangular parallelepiped in a computational space and then a uniform grid is generated there. The Euler equations are solved by the finite volume method using the Runge-Kutta type scheme of the second order accuracy and the local time step technique. Three examples are presented to show the utility of the numerical procedure. Numerical results obtained by the procedure are compared with experimental results and numerical results by the NAL utility code YOKUDO-P based on the full potential equation, and it is shown that the obtained results are in good agreement with the experimental data.

概　　要

翼胴結合体まわり非粘性圧縮遷音速流をEuler方程式に基づいて数値解析するための計算法を提示する。結合体表面や無限遠等における境界条件を正確に取り入れるために結合体外部を計算空間の直方体内部に写像し，そこで一様格子を形成する。Euler方程式は二次精度のRunge-Kutta時間積分スキームと局所時間刻み技法を組入れた有限容積法によって解かれる。この計算法の有効性は三つの計算例によって実証される。得られた結果は，風洞試験の結果やコードYOKUDO-Pによる完全ポテンシャル流の解析結果と比較検討される。

なお，本論文は航空宇宙技術研究所報告TR-896を要約したものである。但し，計算結果の比較にはTR-881の完全ポテンシャル流解析による結果が付記される。

I. INTRODUCTION

In designing either transonic or supersonic aircrafts with the maximum efficiency under the minimum energy consumption there is a strong need for computational analysis to estimate drag, lift, pressure distributions on surface, etc. for various aircraft configurations and flying conditions. In the near future, these computations will be made possible even for the complex configurations owing to remarkable development of computer performance. For numerical analysis of flow about a wing-fuselage combination, several codes[1),2)] to solve the full potential equation have been developed, but they have inherent limitation that isoentropy property obscures the position and the strength of a shock wave. Then, the numerical analysis based on the Euler equa-

* Received April 2, 1986
** Computer Center

tions is regarded to be attractive. Favorably, recent progress in computer performance has made it possible to compute the flowfields about the combinations by solving the Euler equations.

Rizzi[3], Schmidt-Jameson-Whitfield[4),5)], and Agarwal-Deese[6] have solved the Euler equations around the wing-fuselage combinations by the finite volume method. In their analysis, artificial viscosity of filter type is used in order to keep the stability of computation, that is, to suppress appearance of unwanted phenomena in the process of capturing a flow discontinuity. Their results are equally better than that of full potential equation with regard to the position and the structure of shock wave. Their computations are performed by using the grids made by Eriksson[7], Yu[8], and Chen-Caughey-Verhoff[9], with numbers of grid points 64 × 14 × 14, 80 × 16 × 16, and 88 × 16 × 18, respectively. Those numbers of the grid points are too poor to make sufficient comparison with the experimental data of wind tunnel. They have compared the pressure distribution with experimental data only on wing surface but not on fuselage surface.

In this paper we capture the flowfields about the wing-fuselage combinations by solving the three-dimensional Euler equations using the finite volume method combined with the time integration of Runge-Kutta type and the local time step technique. Nature of artificial viscosity added to the equations is the most essential subject in solving the Euler equations. Considering that the dispersion term of filter type used by Rizzi et al. makes the solutions too smooth, we use the artificial viscosity of third order, which is derived taking account of the eigenvalues of amplification matrix of scheme, and the forth order dissipative terms of filter type. We use the computational grid of 176 × 24 × 32 points generated by the NAL utility code YOKUDO-G[10] applying analytical mapping technique. Numerical simulations are carried out for three wing-fuselage combinations, and the obtained pressure distributions are compared with the results of full potential flow by the NAL utility code YOKUDO-P[2] and the experimental data not only on wing serface but also on fuselage surface.

This paper is a summary of Technical Report of National Aerospace Laboratory TR-896 in Japanese, except that this paper includes numerical results of full potential flow in TR-881 for comparisons.

II. GOVERNING EQUATIONS

The three dimensional Euler equations in conservative form are written in Cartesian coordinates as follows.

$$\partial U/\partial t + \partial H^x/\partial x + \partial H^y/\partial y + \partial H^z/\partial z = 0 \tag{1}$$

where the variables U and the fluxes H^x, H^y, and H^z are defined by

$$U = \begin{bmatrix} \rho \\ \rho u \\ \rho v \\ \rho w \end{bmatrix}, \quad H^x = \begin{bmatrix} \rho u \\ \rho u^2 + p \\ \rho uv \\ \rho uw \end{bmatrix},$$

$$H^y = \begin{bmatrix} \rho v \\ \rho vu \\ \rho v^2 + p \\ \rho vw \end{bmatrix}, \quad H^z = \begin{bmatrix} \rho w \\ \rho wu \\ \rho wv \\ \rho w^2 + p \end{bmatrix}.$$

The usual notations are used with u, v, and w as the velocity components, ρ as the density, and p as the pressure.

The energy equation is, assuming steady flow of total enthalpy constant.

$$p = \{(\gamma-1)/\gamma\}\rho[1/2+1/\{(\gamma-1)M_\infty^2\}-(1/2)q^2].$$

Here γ is the specific heat ratio (= 1.4), and the following relations are used:

$$q^2 = u^2 + v^2 + w^2, \; q \equiv (u, v, w),$$
$$c^2 = \gamma p/\rho, \; M = q/c, \; C_p = 2\{p - 1/(\gamma M_\infty^2)\},$$

where M is the Mach number, c the sound velocity, and C_p the pressure coefficient, respectively. The subscript (∞) denotes the value of free-stream.

The governing equations of our computation by the finite volume method are the following ones in integral form deduced by the Gauss divergence theorem from Eqs. (1).

$$(\partial/\partial t) \iiint_V U\,dV + \iint_S (\boldsymbol{H}\cdot\boldsymbol{n})\,dS = 0 \quad (2)$$

where $\boldsymbol{H} \equiv (H^x, H^y, H^z)$, $\boldsymbol{H}\cdot\boldsymbol{n} = H^x n^x + H^y n^y + H^z n^z$, and $\boldsymbol{n} = (n^x, n^y, n^z)$. The V, S, and n denote the volume of an arbitrary cell, the closed surface of the cell, and the unit outer normal vector of the surface, respectively.

III. COMPUTATIONAL SPACE

A grid is generated by the code YOKUDO-G, which is based on the analytical technique and is constructed by a series of mappings; the conformal mapping proposed for flow in a wind tunnel by Caughey, $x + i\theta = \ln\{1-\cosh(\xi + i\eta)\}$ (see reference[11] for detail), is used as a main mapping. Let us consider a symmetrical wing-fuselage combination, and locate its symmetrical plane on x-y plane of $z = 0$ in physical space (see Fig. 1). Since we treat only the case without biased flow, the computations are performed only in $z \geqq 0$ region. In order to treat precisely the boundary conditions on the wing and fuselage surface, symmetrical plane, and at infinity, a computational grid is generated to fit to those boundaries. Fig. 1 shows the correspondence between the physical space and the computational space. The computational space is defined so that the integer values of coordinate point (X, Y, Z) coincide with the coordinates of grid space (I, J, K). Now, our problem to calculate flow about the wing-fuselage combination under the provided Mach number M_∞ and angle of attack α is summarized as follows: Obtain an asymptotically steady solution of Eqs. (2) that satisfies the whole boundary conditions (slip condition, infinity or far field condition, and cyclic condition) on the surface of rectangular parallelepiped.

IV. NUMERICAL PROCEDURE

The three-dimensional Euler equations are solved by finite volume method combined with the time integration of Runge-Kutta scheme and the local time step technique. Here, we briefly describe the numerical methods used in the following (see reference[12] for detail).

Numerical Scheme

For each hexahedronal grid cell in physical space, the governing equations (2) are approximated using the mean value theorem as

$$V_{i,j,k}\,(\partial U/\partial t)_{i,j,k} + \delta\,[\boldsymbol{H}\cdot\boldsymbol{S}]_{i,j,k} = 0, \quad (3)$$

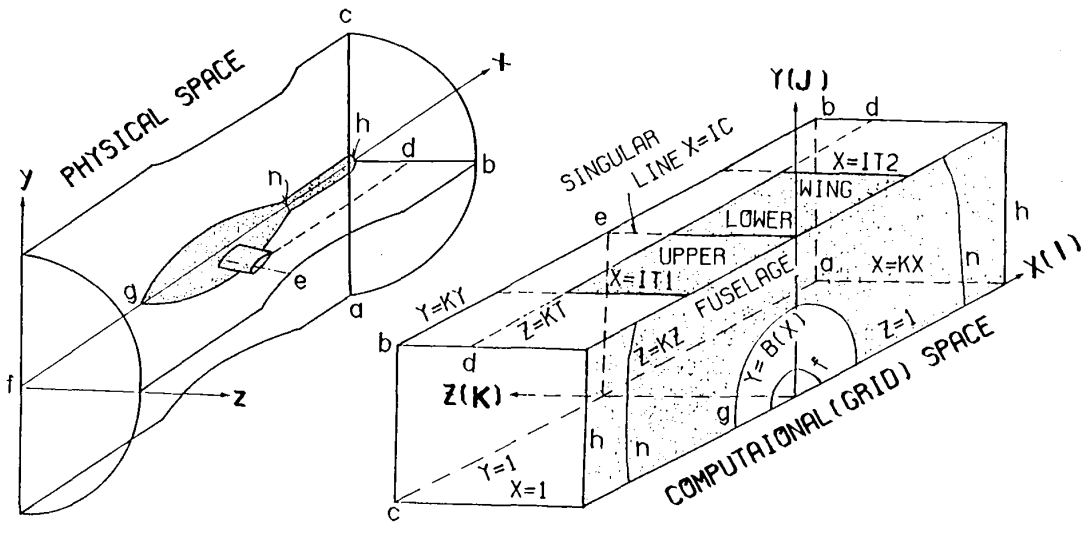

Fig. 1 Correspondence between physical space and computational space

$$\begin{aligned}\delta[H\cdot S]_{i,j,k} \equiv & H_{I+1,j,k}\cdot S^X_{I+1,j,k} - H_{I,j,k}\cdot S^X_{I,j,k} \\ & + H_{i,J+1,k}\cdot S^Y_{i,J+1,k} - H_{i,J,k}\cdot S^Y_{i,J,k} \\ & + H_{i,j,K+1}\cdot S^Z_{i,j,K+1} - H_{i,j,K}\cdot S^Z_{i,j,k}\end{aligned} \tag{4}$$

where the suffices i, j, and k denote the positions corresponding to $X = I+1/2$, $Y = J+1/2$, and $Z = K+1/2$, respectively. V denotes the volume of the cell, and S^X, S^Y, and S^Z are the area vectors in the direction of X, Y, and Z, respectively (see Fig. 2). In the finite volume method, the value U at the center of the cell is approximately calculated by integrating Eqs. (3) in time direction with a method described in the next section.

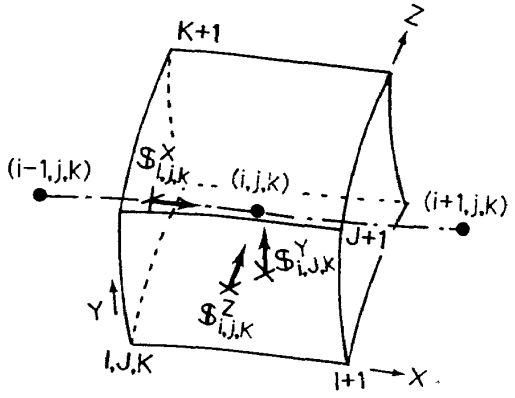

Fig. 2 Grid cell and area vectors in physical space

The Runge-Kutta Integral Scheme

We use the following Runge-Kutta scheme[3] of the second order accuracy. Let the solution of N step, $U^N_{i,j,k}$, be known, then the solution of $N+1$ step is calculated with the following procedure.

$$\begin{aligned}\tilde{U}^{(1)} &= U^N - (\Delta t/V)\,\delta\,[H^N\cdot S] \\ \tilde{U}^{(2)} &= U^N - (\Delta t/2V)\{\delta\,[H^N\cdot S] + \delta\,[\tilde{H}^{(1)}\cdot S]\} \\ \tilde{U}^{N+1} &= U^N - (\Delta t/2V)\{\delta\,[H^N\cdot S] + \delta\,[\tilde{H}^{(2)}\cdot S]\}\end{aligned} \tag{5}$$

where $\tilde{H}^{(L)} \equiv H(\tilde{U}^{(L)})$, $(L = 1, 2)$, and $H^N \equiv H(U^N)$.

Local Time Step Technique

The aim of this paper is to obtain a steady flow, and the local time step technique is applied to increase the rate of convergence of a solution. From the von Neumann's analysis of stability for the above scheme, the condition of stability for an increment of time is given as, (see reference[12])

$$\Delta t \leqq \frac{2V}{(1+1/\gamma)(Q^X+Q^Y+Q^Z)/2 + \{(1-1/\gamma)^2(Q^X+Q^Y+Q^Z)^2 + (4c^2/\gamma)[S]\}^{1/2}} \equiv \Delta T),$$

where $Q^\kappa \equiv |q\cdot S^\kappa|$, $(\kappa = X, Y, Z)$, and $[S] \equiv S^X\cdot S^X + S^Y\cdot S^Y + S^Z\cdot S^Z + 2(|S^X\cdot S^Y| + |S^Y\cdot S^Z| + |S^Z\cdot S^X|)$. In the local time step technique, for each grid cell ΔT is calculated and $\Delta t_{i,j,k} = C_{\Delta T} \times \Delta T_{i,j,k}$ (the coefficient $C_{\Delta T} \sim 1$) is used in Eqs. (5).

Artificial Viscosity and Numerical Dissipative Term

If computation for one step is repeated by the above scheme, numerical oscillations may generate in regions of large gradients of physical variables, such as a shock wave region. To damp the oscillations we use the third order artificial viscosity and the forth order numerical dissipative terms. Adding the artificial viscosity to $\tilde{U}^{N+1}$ of Eqs. (5), we obtain

$$\begin{aligned}\hat{U}^{N+1} = \tilde{U}^{N+1} &+ (\Delta t/\Delta X)\lambda^X \partial/\partial X(|\partial U^X/\partial X|^N \partial U^N/\partial X)(\Delta X)^3 \\ &+ (\Delta t/\Delta Y)\lambda^Y \partial/\partial Y(|\partial U^Y/\partial Y|^N \partial U^N/\partial Y)(\Delta Y)^3 \\ &+ (\Delta t/\Delta Z)\lambda^Z \partial/\partial Z(|\partial U^Z/\partial Z|^N \partial U^N/\partial Z)(\Delta Z)^3\end{aligned} \tag{6}$$

where λ^X, λ^Y, and λ^Z are the coefficients of artificial viscosity of O(1), and $U^\kappa \equiv (\Delta\kappa/V) \times (uS^{\kappa x} + vS^{\kappa y} + wS^{\kappa z})$, $(\kappa = X,Y,Z)$. These U^κ are the basic variables whose polynomials constitute[12] the eigenvalues of amplification matrix of scheme presented in the above section. Finite difference approximation for a part of X term in RHS of (6) is written as

$$\{\partial/\partial X\,(|\partial U^X/\partial X\,|\partial U/\partial X)\}^N_{i,j,k} \sim \{|U^X_{i+1} - U^X_i|\,(U_{i+1} - U_i) - |U^X_i - U^X_{i-1}|(U_i - U_{i-1})\}^N_{*,j,k},$$

$$S^{Xx}_{i,j,k} \sim (1/2)(S^{Xx}_{I+1} + S^{Xx}_I)_{*,j,k}.$$

The other components in Y and Z directions are also approximated in finite difference forms similar to the above.

Further we use numerical dissipative terms to make the computation more stable. The numerical dissipative terms are added to the solution $\hat{U}^{N+1}$ as

$$U^{N+1} = \hat{U}^{N+1} - \epsilon^X(\partial^4 U^N/\partial X^4)(\Delta X)^4 - \epsilon^Y(\partial^4 U^N/\partial Y^4)(\Delta Y)^4 - \epsilon^Z(\partial^4 U^N/\partial Z^4)(\Delta Z)^4,$$

where ϵ^κ $(\kappa = X,Y,Z)$ are coefficients and the finite difference approximation such as the following is used.

$$(\partial^4 U/\partial X^4)_i = (U_{i+2} - 4U_{i+1} + 6U_i - 4U_{i-1} + U_{i-2})/(\Delta X)^4$$

In computation we set $\lambda^\kappa = 0.2$, $\epsilon^\kappa = 0.01$, $(\kappa = X, Y, Z)$ from our experience.

Boundary Conditions

In the finite volume method, the boundary conditions are included in the expression of the flux $\boldsymbol{H}$ (Eqs. (4)). Each cell has six faces, and if a face is shared by two cells, then the value of $\boldsymbol{H}$ on the face is given by the average of ones at the center of two cells.

On the cell face coinciding with the body surface or the symmetric plane, the vlaue of $\boldsymbol{H}\cdot\boldsymbol{S}^\kappa$ $(\kappa = Y$ or $Z)$ is obtained from the slip condition; for example on the face of $K = 1$, the flux in Z direction is obtained as

$$\boldsymbol{H}\cdot\boldsymbol{S}^Z = \begin{bmatrix} 0 \\ pS^{Zx} \\ pS^{Zy} \\ pS^{Zz} \end{bmatrix}, \quad \text{where } \boldsymbol{S}^Z \equiv \begin{bmatrix} S^{Zx} \\ S^{Zy} \\ S^{Zz} \end{bmatrix},$$

from the condition $\boldsymbol{q}\cdot\boldsymbol{S}^Z = 0$. Here p is calculated by solving the following equation[12]:

$$\partial p/\partial Z = (1/|\boldsymbol{S}^Z|^2)\,[\rho\{(\boldsymbol{q}\cdot\partial\boldsymbol{S}^Z/\partial X)(\boldsymbol{q}\cdot\boldsymbol{S}^X) + (\boldsymbol{q}\cdot\partial\boldsymbol{S}^Z/\partial Y)(\boldsymbol{q}\cdot\boldsymbol{S}^Y)\} - (\boldsymbol{S}^Z\cdot\boldsymbol{S}^X)\partial p/\partial X - (\boldsymbol{S}^Z\cdot\boldsymbol{S}^Y)\partial p/\partial Y]$$

As the singular line before the nose of fuselage in physical space corresponds to a part of $K = 1$ plane in the computational space, on the cell face coinciding with this, we impose $\boldsymbol{H}\cdot\boldsymbol{S}^Z = 0$.

A cell face on $J = KY$ corresponds to either the wing surface or an inner face in physical space, and on the latter face the cyclic condition is imposed and the flux is given by

$$[\boldsymbol{H}\cdot\boldsymbol{S}^Y]_{i,J=KY,k} \sim (1/2)(\boldsymbol{H}_{i,j=NY,k} + \boldsymbol{H}_{i^*,j=NY,k})\cdot\boldsymbol{S}^Y_{i,J=KY,k}$$

where $i^* = KX + 1 - i$, and $NY = KY - 1$ (see Fig. 1).

On the cell face of the upperstream boundary the freestream condition $\boldsymbol{H} = \boldsymbol{H}_\infty$ is assumed. For the downstream boundary, the flux $\boldsymbol{H}$ is calculated by the following ρ and $\boldsymbol{q}$, which are obtained from the introduction of the Riemann invariants (R) for a one-dimensional flow normal to the boundary of grid after Jameson-Baker[13],

$$\rho = \{(\gamma-1)(R_e - R_\infty)/(4c_e)\}^{2/(\gamma-1)}\rho_e$$
$$\boldsymbol{q} = \boldsymbol{q}_e + \{(R_e + R_\infty)/2 - \tilde{\boldsymbol{n}}\cdot\boldsymbol{q}_e\}\tilde{\boldsymbol{n}}$$

where

$$c_e^2 = (\gamma-1)\,[1 + 2/\{(\gamma-1)M_\infty^2\} - \boldsymbol{q}_e^2]/2,$$
$$R_e = \boldsymbol{q}_e\cdot\tilde{\boldsymbol{n}} + 2c_e/(\gamma-1),$$

$$R_\infty = \boldsymbol{q}_\infty \cdot \tilde{\boldsymbol{n}} - 2c_\infty/(\gamma - 1),$$
$$\tilde{\boldsymbol{n}} = S^X_{KX,j,k}/|S^X_{KX,j,k}|$$

and the suffix (e) denotes the value extrapolated from the interior cells adjacent to the boundary.

V. NUMERICAL RESULTS

Using the abovementioned procedure the numerical experiments were successfully performed for several wing-fuselage combinations under various (α, M_∞) conditions, and it took about 1.5 ~ 4 hours for each case on FACOM M-380 computer. The grid was generated by the code YOKUDO-G, and in order to increase the efficiency of computation we prepared three successively refined grids for each case. At first the computation was performed in the coarse grid under the initial condition of freestream flow, and it was succeeded by the computation in the medium grid. At last, using the results interpolated in the fine grid (176 X 24 X 32) as the initial flow, the asymtotically steady solution was obtained after several hundred cycles. In this paper we show three numerical examples.

1) Combination of Cylinder and ONERA-M6 Wing

The computation was carried out for the ONERA-M6[14] wing attached to the lower part of cylinder at $M_\infty = 0.84$ and $\alpha = 3.06°$. The grid, and the isobaric contours and sonic lines on the surface of wing-cylinder combination are shown in Fig. 3. The result of full potential computation is also shown to compare with that of the Euler equations. The triple shock wave which is the phenomenon peculiar to transonic flow around a swept wing is captured by both equations, however, it is known that the forward shock wave located in inner part of upper wing surface, which is the oblique shock wave from

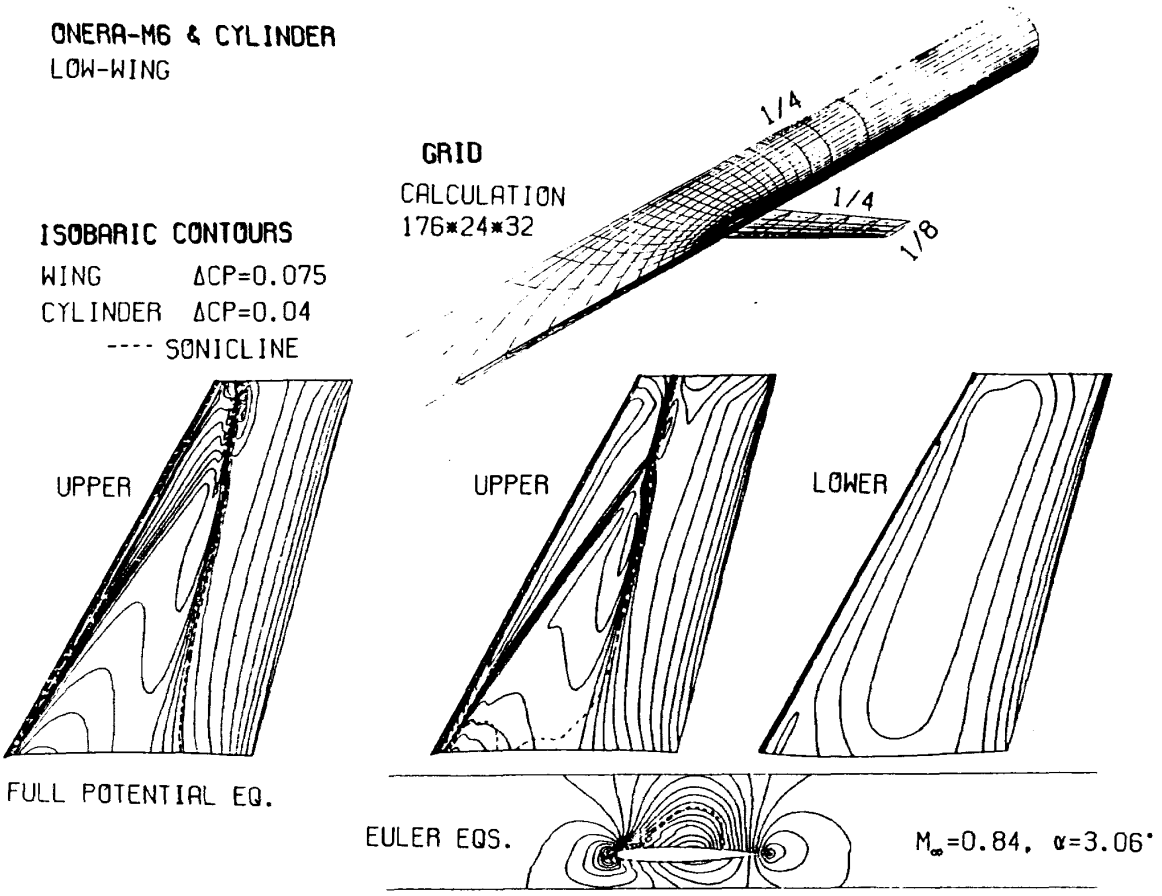

Fig. 3 Grid and isobaric contours on surfaces of cylinder and ONERA-M6 wing combination

supersonic to supersonic, is captured more clearly in the result of the Euler equations than that of full potential equation. The three-pronged part of triple shock wave is also clear in the result of the Euler equations.

2) RAE-$W_A B_2$(0)0 Wing-Fuselage Combination

The computation was carried out for the y-symmetrical RAE-$W_A B_2$(0)0 Wing-fuselage combination at $M_\infty = 0.8$ and $\alpha = 0°$. The grid on the surface of combination is shown in Fig. 4. Fig. 5 shows the pressure coefficients on surface of wing, and the present results are compared with the experimental data given by Treadgold et al.,[15] and with the numerical results by the full potential code YOKUDO-P. In this case the good agreement between these results are obtained by reason of no shock wave in flowfield. Also, Fig. 6 shows the comparison among three results with regard to the pressure coefficients on the meridians of the fuselage surface. It is clear that the present results agree well with the experimental results in almost all, however, in full potential results the difference from the experimental data near the leading edge spreads from the junction of wing-fuselage to the symmerical plane ($\theta = \pm 90°$). Treadgold et al.[15] have shown five experimental data besides the present case,

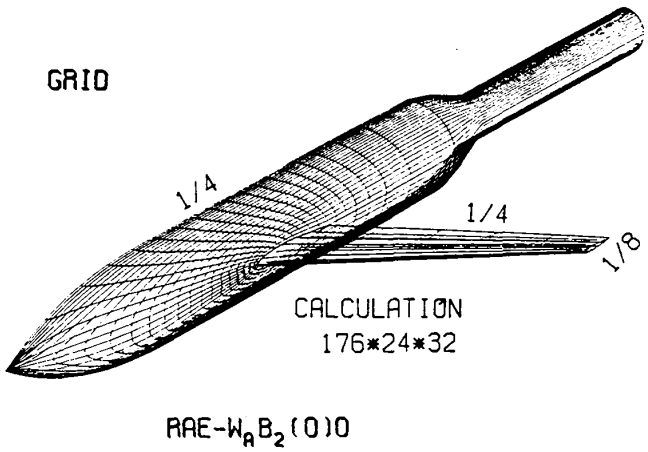

Fig. 4 Grid of RAE $W_A B_2$ (0)0 wing-fuselage combination

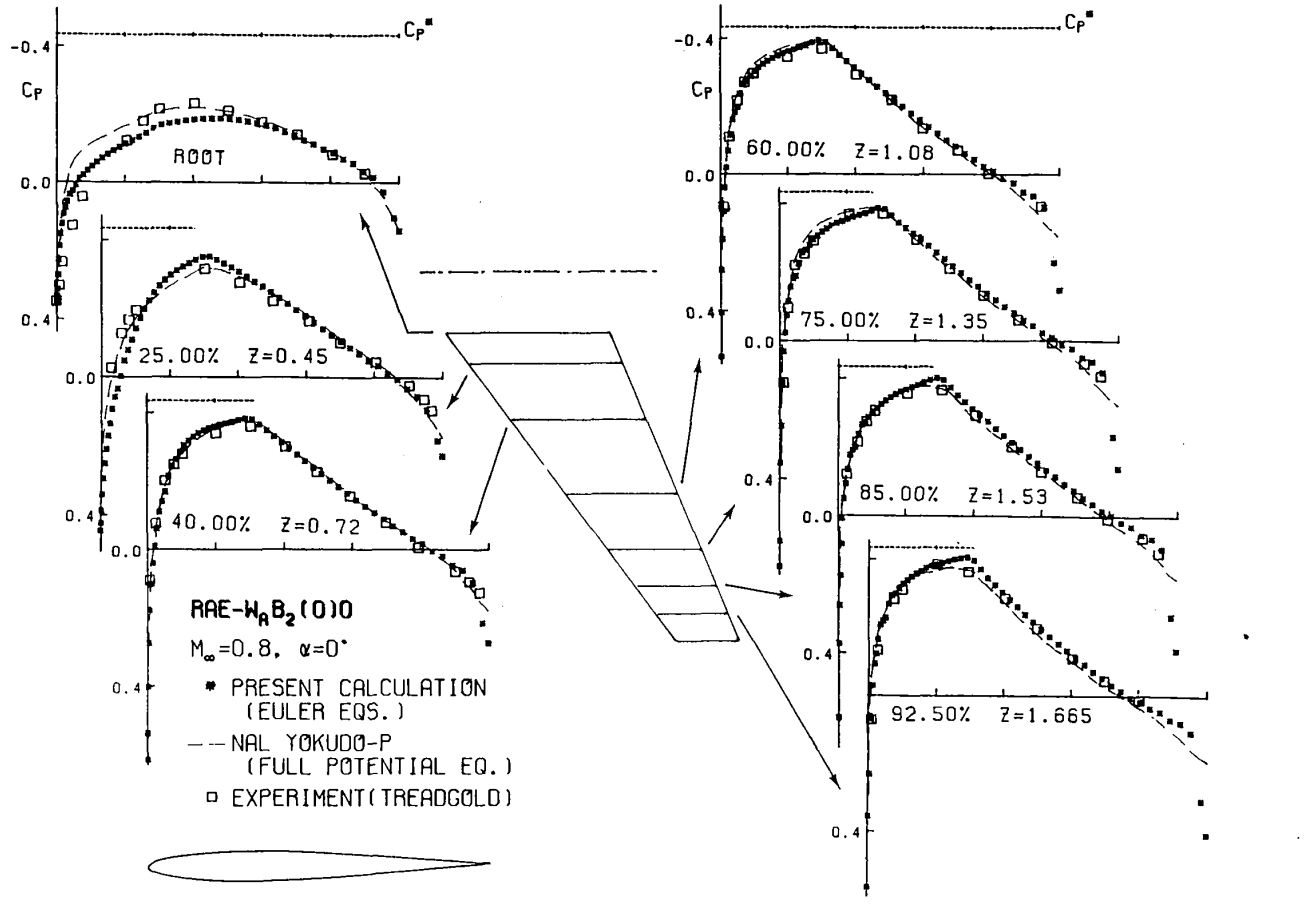

Fig. 5 C_p-distribution on wing surface of RAE $W_A B_2$ (0)0

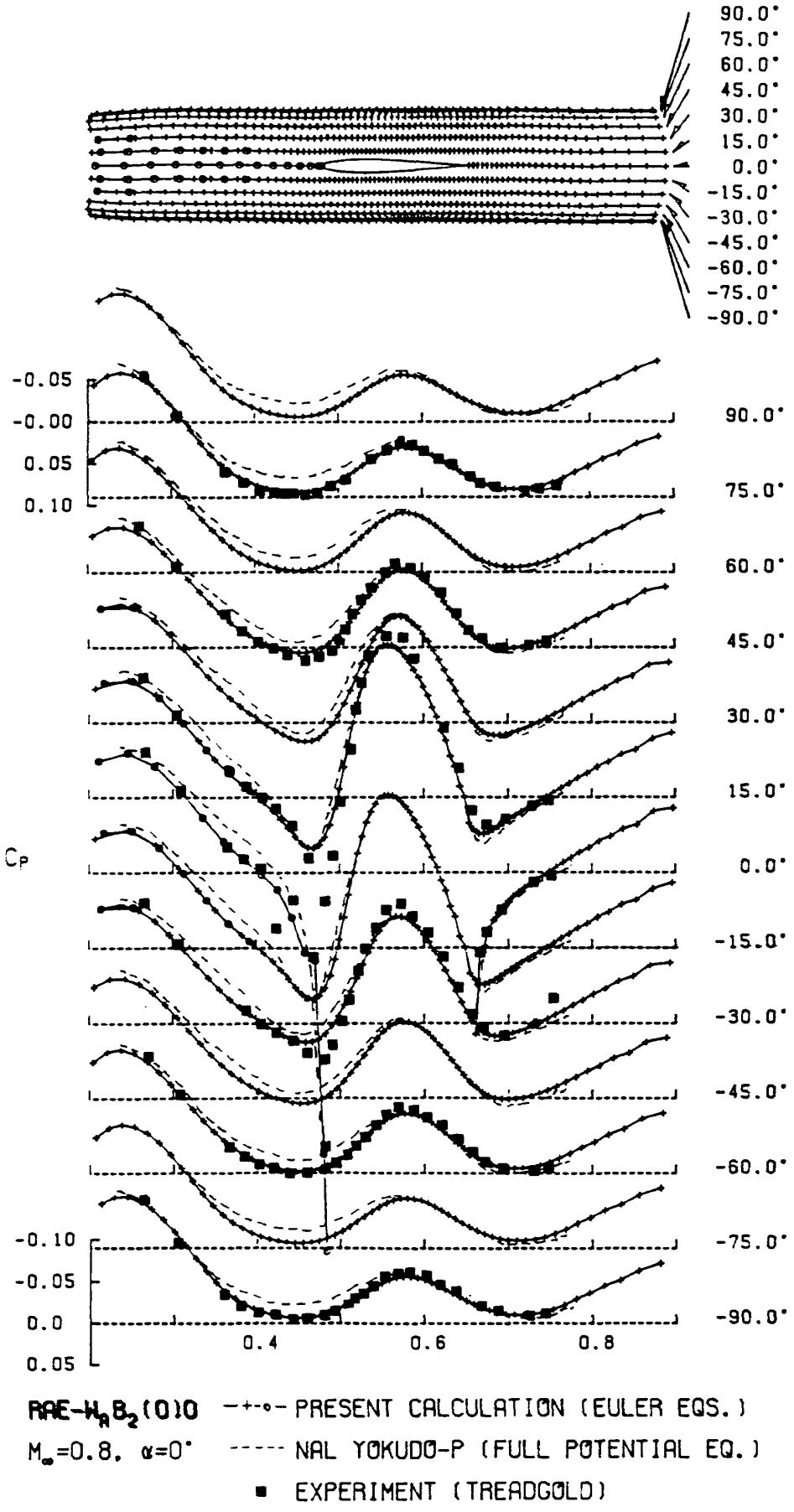

Fig. 6 C_p-distribution on fuselage surface of RAE $W_A B_2$ (0)0

and our results by the present numerical procedure based on the Euler equations agree well with the experimental data (see reference[12]).

3) NAL-720211 Wing-Fuselage Combination

In this section we have solved the flowfields around the NAL-720211 wing-fuselage combination that is similar to the real aircraft at M_∞ = 0.792 and α = 2.462°. The grid is shown in Fig. 7. Figure 8 shows the isobaric contours on the surfaces of wing and fuselage, where the triple shock is observed on the upper surface of wing. Figure 9 shows the result of present computation, that by full potential code, and experimental data of NAL[16] with regard to pressure distributions on the surface of the wing. From the figure, the oblique shock wave near 20 ~ 40% chord, which is the shock wave from supersonic to supersonic, is clearly calculated by the present procedure and is caught in experimental data but cannot be caught by full potential code. For the strong shock wave from supersonic to subsonic

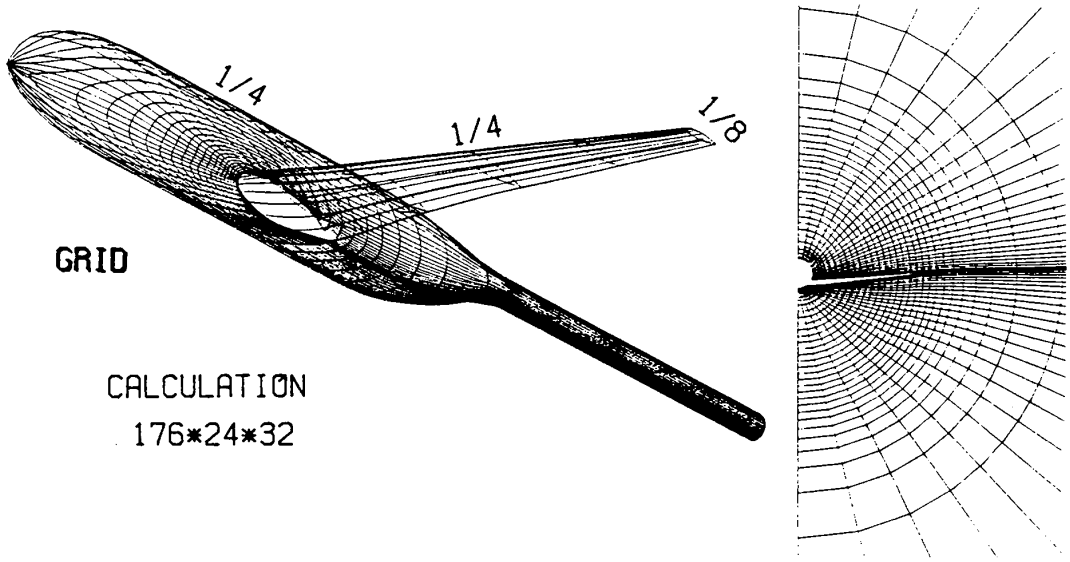

Fig. 7 Grid of NAL-720211 wing-fuselage combination

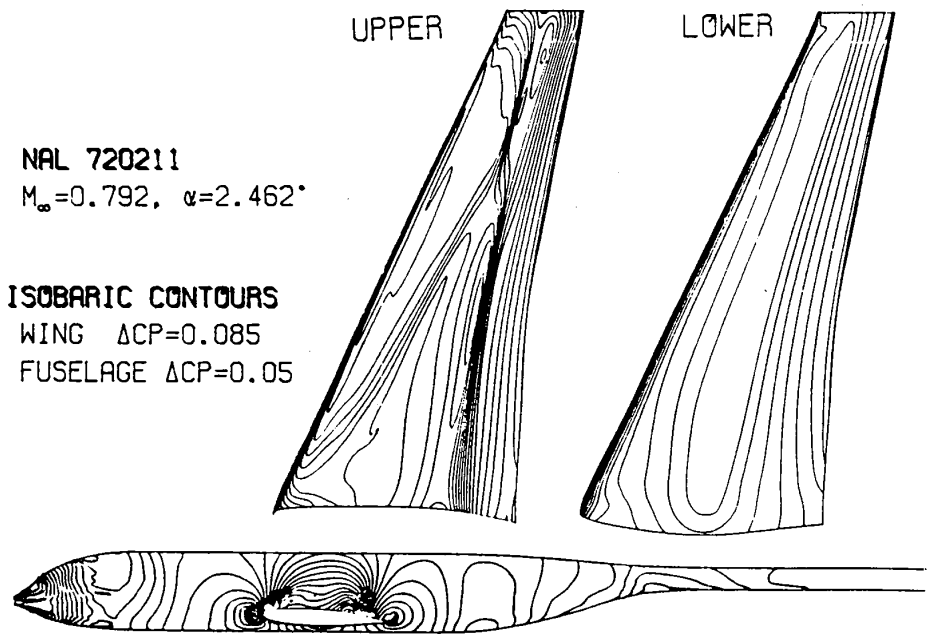

Fig. 8 Isobaric contours obtained by using the Euler equations

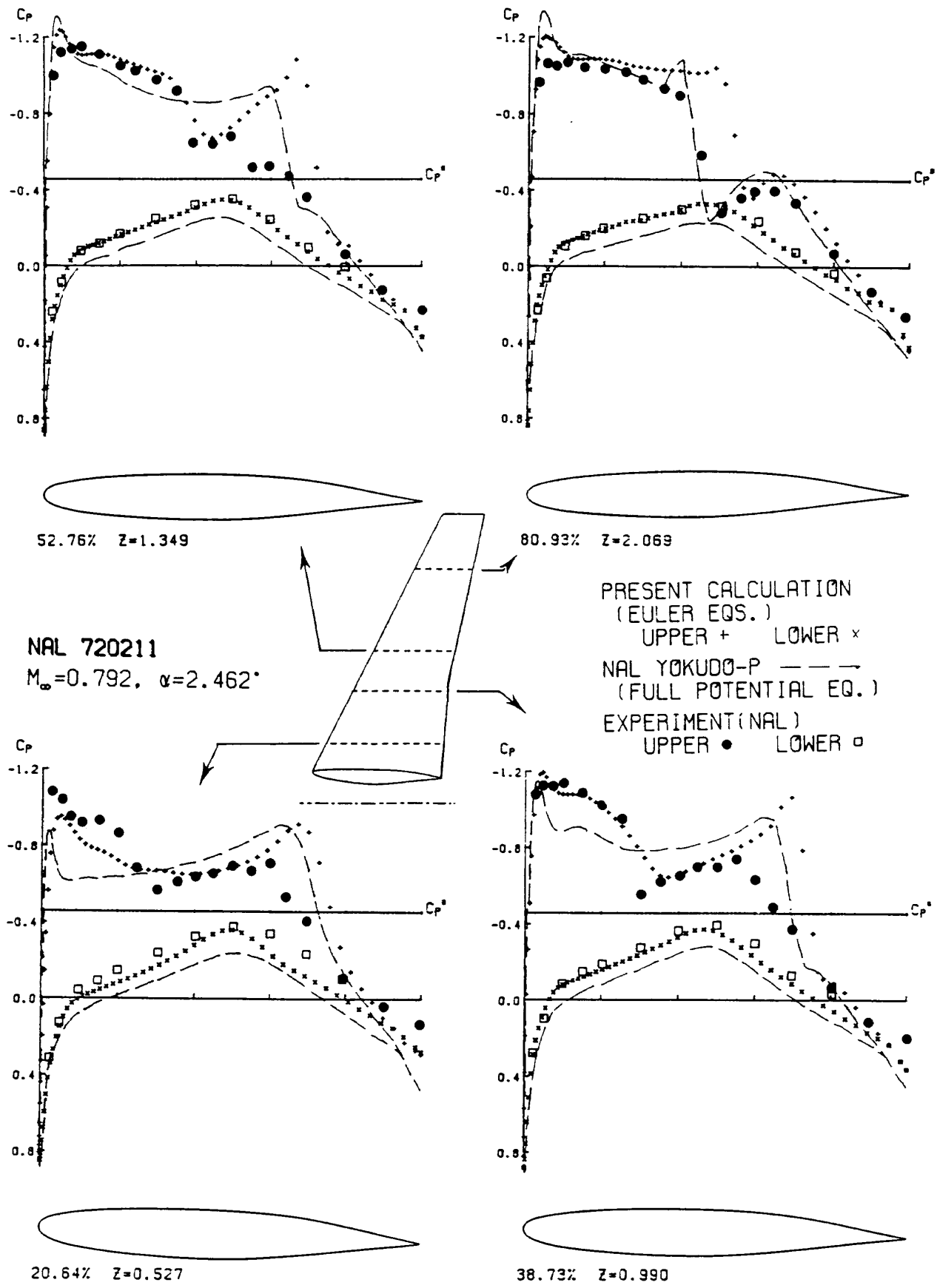

Fig. 9 C_p-distribution on wing surface of NAL-720211

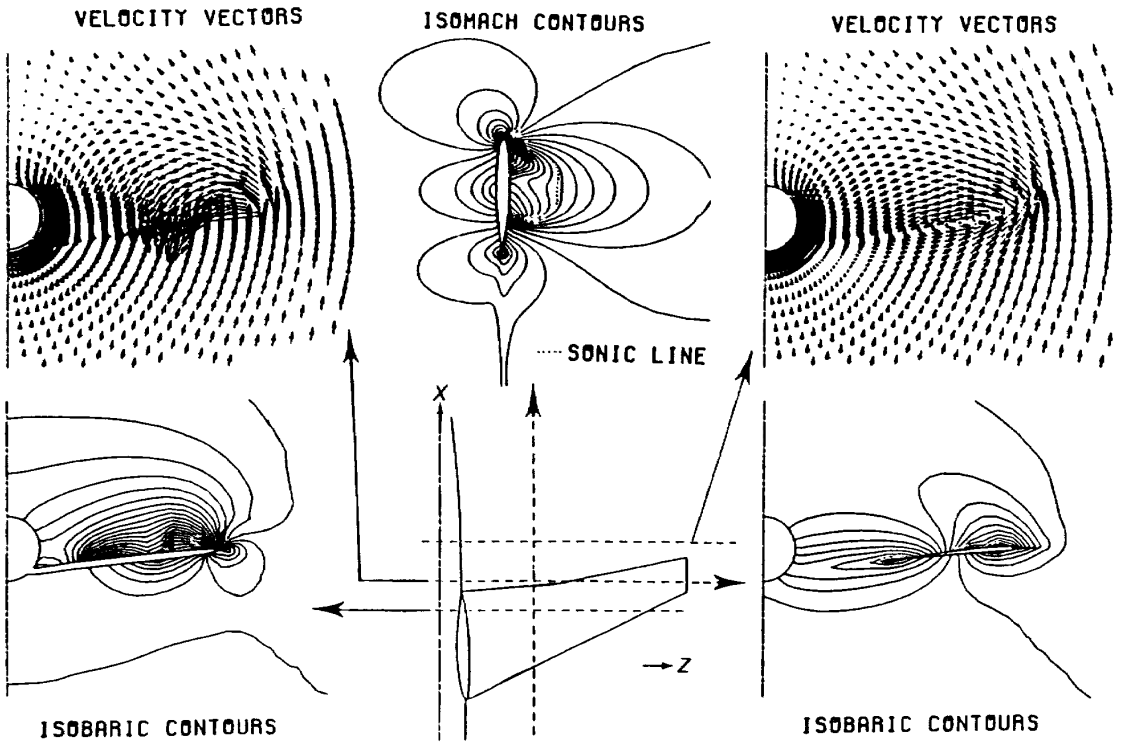

Fig. 10 Flowfields of y-z velocity vectors, Iso-Mach contours, or Isobaric contours on four cutting planes

near 50 ~ 80% chord, the pressure jump of our result is larger than that of experimental data, and this discrepancy is caused by the effect of the separation of flow near the boundary layer. The visualization of the result is the most important subject in the computation of three-dimensional complex flowfield. By our computational code the flowfield on an arbitrarily cutting plane can be visualized, and Fig. 10 shows the projective velocity vectors, iso-Mach contours, and isobaric contours on the cutting planes defined by y axis and the broken lines. From the figure we can easily observe a double shock wave inside of a sonic line on the z = constant plane and vortex flow on x = constant plane in downstream region of the trailing edge, etc.

VI. CONCLUSIONS

In this paper we have presented a numerical procedure to solve the three-dimensional Euler equations around wing-fuselage combination in transonic flow. The computational grid was generated by the NAL utility code YOKUDO-G, and the Euler equations were solved by the finite volume method combined with the Runge-Kutta time integral scheme of the second order accuracy and the local time step technique. The third order artificial viscosity, which was derived taking account of the eigenvalues of amplification matrix, was used to stabilize the numerical oscillation.

We have executed the numerical experiments for several wing-fuselage combinations under various conditions to examine the validity of our procedure, and in this paper the results of three cases have been presented. It is clear that our result in each case is adequate comparing with the experimental data of wind-tunnel or the numerical results of full potential equation. Especially, we have clearly captured the oblique shock wave from supersonic to supersonic which is obscure in the numerical calculation of full potential equation.

Though we have shown the method to solve the Euler equations, the Navier-Stokes equations

can be also solved by the similar procedure including the viscosity terms and the equation of total energy. As the grid was still coarse in our computation, the detailed structure of vortices near the wing tip could not be captured. However, in a year or two more precise computation will be performed using a super computer, and then the more detailed structure of flow around such a large scale body as a wing-fuselage combination will be easily analyzed. Considering the scale of wing-fuselage combinations and the limitation of computer advancement, the numerical analysis based on the Euler equations will play a very important role in the development of aircrafts in the near future.

ACKNOWLEDGEMENTS

The authors would like to express their sincere gratitude to Kohei Suetsugu, Sanko Software Development Ltd., for his assistance in their work.

REFERENCES

1) D.A. Caughey and A. Jameson; Progress in Finite Volume Calculations for Wing-Fuselage Combinations, *AIAA J.*, **18**, No. 11 (1980) pp. 1281-1288.
2) T. Ishiguro; Numerical Analysis of Inviscid Flows about Wing-Fuselage Combination, II. Development of Full Potential Flow Code YOKUDO-P, NAL TR-881 (1985), (in Japanese).
3) A. Rizzi; Damped Euler-Equation Method to Compute Transonic Flow Around Wing-Body Combinations, *AIAA J.*, **20**, No. 10 (1982) pp. 1321-1328.
4) W. Schmit, A. Jameson & D. Whitfield; Finite Volume Solution for the Euler Equation for Transonic Flow over Airfoils and Wings Including Viscous Effects, AIAA Paper 81-1265 (1981).
5) W. Schmit, A. Jameson & D. Whitfield; Finite Volume Solutions to the Euler Equations in Transonic Flow, *J. Aircraft*, **20**, No. 2 (1983) pp. 127-133.
6) R.K. Agarwal & J.E. Deese; Transonic Wing-Body Calculations Using Euler Equations, AIAA Paper 83-0501 (1983).
7) L.E. Eriksson; Generation of Boundary-Conforming Grid Around Wing-Body Configurations Using Transfinite Interpolation, *AIAA J.*, **20**, No. 10 (1982) pp. 1313-1320.
8) N.J. Yu; Grid Generation and Transonic Flow Calculations for Three-Dimensional Configurations, AIAA Paper 80-1391 (1980).
9) L-T. Chen, D.A. Caughey & A. Verhoff; A Nearly Conformal Grid-Generation Method for Transonic Wing-Body Flowfield Calculations, AIAA Paper 82-0108 (1982).
10) T. Ishiguro, N. Kamiya & K. Oguchi; Numerical Analysis of Inviscid Flows about Wing-Fuselage Combination, I. Development of Grid Generation Code YOKUDO-G, NAL TR-864 (1985), (in Japanese).
11) D.A. Caughey; A Systematic Procedure for Generating Useful Conformal Mapping, *Int. J. Numerical Methods in Engineering*, **12** (1978) pp. 1651-1657.
12) T. Ishiguro, S. Ogawa & K. Oguchi; Numerical Analysis of Inviscid Flows about Wing-Fuselage Combination, III. Calculation based on the Euler Equations, NAL TR-896 (1985), (in Japanese).
13) A. Jameson & T.J. Baker; Solution of the Euler Equations for Complex Configurations, AIAA Paper 83-1929 (1983).
14) B. Monnerie & F. Charpin; Essais de Buffeting dúne Aile en Fleche en Transsonique, 10^{e} Colloque d'Aérodynamique Appliquee, No. V, (1973).
15) T.A. Treadgold, A.F. Jones & K.H. Wilson; Pressure Distribution Measured in the RAE 8 ft × 6 ft Transonic Wind Tunnel on RAE Wing 'A' in Combination with an Axi-Symmetric Body at Mach Number of 0.4, 0.8 and 0.9, Experiment Data Base for

Computer Program Assessment, AGARD-AR-138 (1979).

16) N. Kamiya; National Aerospace Laboratory, 1985, private communication.

TECHNICAL REPORT OF NATIONAL
AEROSPACE LABORATORY
TR-896T

航空宇宙技術研究所報告896T号（欧文）

昭和61年5月発行

発行所　航空宇宙技術研究所
東京都調布市深大寺東町7丁目44番地1
電話武蔵野三鷹(0422)47-5911(大代表)〒182
印刷所　株式会社　東京プレス
東京都板橋区桜川2－27－12

Published by
NATIONAL AEROSPACE LABORATORY
1,880 Jindaiji, Chōfu, Tokyo
JAPAN

Printed in Japan